Feature Based Multi-Hypothesis Map Representation for Localization in Non-Static Environments

Kristin Nielsen and Gustaf Hendeby

Nielsen, K., Hendeby, G., (2022), Feature Based Multi-Hypothesis Map Representation for Localization in Non-Static Environments, *2022 25th International Conference on Information Fusion (FUSION)*. https://doi.org/10.23919/FUSION49751.2022.9841255

Feature Based Multi-Hypothesis Map Representation for Localization in Non-Static Environments

Kristin Nielsen*† and Gustaf Hendeby†
*Epiroc Rock Drills AB; Örebro, Sweden
kristin.nielsen@epiroc.com
†Dept. Electrical Engineering; Linköping University; Linköping, Sweden
gustaf.hendeby@liu.se

***Abstract*—Long-term autonomy of robots requires localization in an inevitably changing environment, where the robots' knowledge about the surroundings are more or less uncertain. Inspired by methods in target tracking, this paper proposes a feature based multi-hypothesis map representation to provide robust localization under these conditions. It is derived how this representation can be used to obtain consistent position estimates while at the same time providing up-to-date map information to be shared by cooperative robots or for visual presentation. Simulations are performed that conceptually highlights the benefit of the developed solution in an environment where uniquely identifiable landmarks are moved between discrete positions. This relates to a real world scenario where a robot moves in a corridor with office doors opened or closed at different times.**

***Index Terms*—multi-hypothesis, localization**

I. Introduction

In robotics, when targeting the problem of position estimation or mapping, it has traditionally been assumed that the environment is static [1]. In reality this is almost never the case, especially not for long-term operations. From a robots perspective an environment subject to change can be categorized into two main categories,

- a *dynamic* environment, containing objects moving relatively fast so that the robot's perception of the object changes while the object is in field-of-view, or,
- a *non-static* environment, where changes in the environment are much slower and typically not captured by the robot's sensors in real time. Changes are rather discovered when the robot re-visits a previously visited area.

This paper proposes a feature based multi-hypothesis map representation for position estimation in a non-static environment inspired by methods in target tracking. Multiple hypotheses of feature locations are allowed in the map and as the robot moves, the currently active hypothesis is selected for processing. In this way, up-to-date information about the environment can be extracted and possibly communicated to cooperative robots, or be used for visualization to a user.

This work was partially supported by the Wallenberg AI, Autonomous Systems and Software Program (WASP) funded by the Knut and Alice Wallenberg Foundation.

Other multi-hypothesis map representations have been presented in the literature. In [2, 3] features are used to build a multi-hypothesis map. However, the different hypothesis originate from uncertainty in the data associations, and the true feature positions are in fact assumed static.

Work not assuming a static environment, using a sample based map representation, can be found in [4, 5] where a randomly selected, fixed fraction, of a 2D range data is replaced each time a place is revisited. In [6] distinct *experiences* from specific places are extracted, where an experience is a temporal sequence of sensor observations associated with a small physical area. A collection of stereo camera frames captured near a single physical location models a place in [7, 8] and a similar approach for 2D lidar is taken in [9].

Another common map representation is the occupancy grid map, for which work on non-static environments can be found in [10] and [11] where the concept of a *dynamical occupancy grid* is proposed independently. In [12] a 3D OctoMap presented in [13] is used, which is a probabilistic 3D occupancy grid map. An occupancy grid map is also used in [14] were they consider incoming observation not matching the current map. Based on the uncertainty in the position of the robot they decide if the map should be updated or not.

A feature based map representation is sensor agnostic and scales better over larger regions than an occupancy grid map. The drawback of feature based maps is the imperfections in the methods used to extract features from raw data. However, these uncertainties can be modeled and the approach presented in this paper accounts for them. In [15] a persistence filter is introduced describing the survival of features over time. This models the memory decay of features not perceived for a long time, but cannot manage different hypothesis of the same landmark. In [16] the spatio-temporal dynamics of the environment is modeled by its frequency spectrum, allowing a good prediction of periodical changes in the environment.

The map representation proposed in this paper includes multiple hypotheses of landmark positions and models the transition between the positions as Markov chains. This map can be used for multi-hypothesis state estimation to provide consistent results in environments where landmarks are moved between discrete positions. This is verified in two simulated

environments, one open space environment conceptually showing the benefit of the developed solution, and a more realistic environment of an office corridor where uniquely identifiable landmarks are placed on the door handles. The doors being opened or closed comprises the different hypotheses.

The probabilistic state estimation problem is formulated in Section II, followed by a presentation of the suggested multi-hypothesis map representation in Section III. Section IV defines a hypothesis test to allow for decisions in the otherwise exponentially growing hypothesis tree, and thereby makes the method computationally tractable. In Section V the multi-hypothesis state estimation algorithm is outlined and Section VI presents the simulation experiments. Concluding remarks are given in Section VII.

II. Probabilistic State Estimation

This section describes state estimation in the probabilistic framework and defines notations used throughout this paper.

The trajectory of a moving robot is described by a sequence of random variables $x_{1:T} = \{x_1, \dots, x_T\}$. System inputs (*e.g.*, odometry measurements) are given by $u_{1:T} = \{u_1, \dots, u_T\}$, and perception of the environment by $z_{1:T} = \{z_1, \dots, z_T\}$. A representation of a map of the operation area is given by $\mathcal{M}$. In a standard localization application the map is assumed known and static over time. With a feature representation it is completely defined by a number of landmarks $\mathcal{M} = \{m_1, \dots m_n\}$.

Solving the filtering state estimation problem consists of estimating the probability $p(x_T|\mathcal{M}, z_{1:T}, u_{1:T})$, which can be solved recursively given a *state transition model*, $p(x_t|x_{t-1}, u_t)$, and an *observation model* $p(z_t|x_t, \mathcal{M})$. The recursive update is usually done in a two-step procedure where a time update,

$$p(x_t|\mathcal{M}, z_{1:t-1}, u_{1:t}) = \int p(x_t|x_{t-1}, u_t) \times p(x_{t-1}|\mathcal{M}, z_{1:t-1}, u_{1:t-1})dx_{t-1}, \quad (1)$$

is followed by a measurement update using Bayes' rule,

$$p(x_t|\mathcal{M}, z_{1:t}, u_{1:t}) = \frac{p(z_t|x_t, \mathcal{M})p(x_t|z_{1:t-1}, \mathcal{M}, u_{1:t})}{p(z_t|z_{1:t-1}, \mathcal{M}, u_{1:t})}. \quad (2)$$

This gives an estimate of the current state given an estimate from the previous time-step, $p(x_{T-1}|\mathcal{M}, z_{1:(T-1)}, u_{1:(T-1)})$.

This problem, with an assumed static environment, is from now on referred to as the static state estimation problem. For linear state transition and observation models, this recursion has an analytic solution in form of the well-known Kalman filter [17]. In the nonlinear case, approximate solutions are available such as the *extended Kalman filter* (EKF), the *unscented Kalman filter* (UKF), or the *particle filter* (PF) [1].

III. Non-Static Environment

Throughout this paper it is assumed that landmarks are uniquely identifiable by the robot's perception system, and the environment is non-static, *i.e.*, landmarks are moved between discrete positions while not in the robot's field-of-view. Under these assumptions, the static representation of the map fails to give good state estimates. If a landmark with a specific signature is moved, the localization system receives observations of that landmark potentially far away from its position in the map, and will compensate for this by erroneously adjusting the state estimate. Fig. 1 depicts an example of this situation when a robot is moving in a corridor with uniquely identifiable landmarks attached to doors that can either be open or closed.

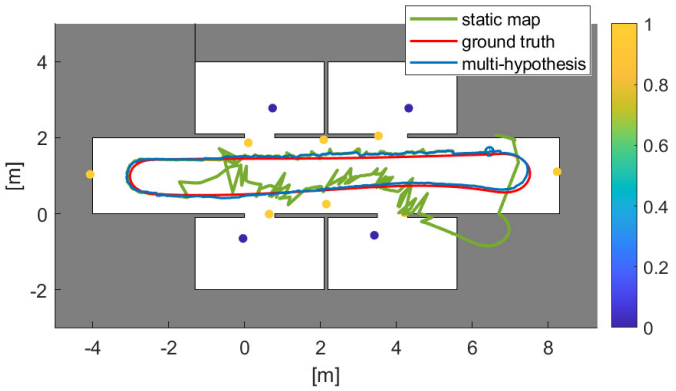

Fig. 1. Trajectory estimates when a robot is moving along a counter clockwise trajectory (red line) in a corridor environment with landmarks placed on walls and door handles. The robot starts to the right with all doors opened and when the robot is in the leftmost position all doors are closed. The green line depicts the trajectory from a static state estimation where landmarks are placed at positions corresponding to open doors in the map and the blue line is from the multi-hypothesis map localization described in Algorithm 1. The color of the landmarks depict their estimated probability of existence at the end of the simulation.

A solution to this is to allow the map to include multiple landmarks with the same signature, representing all possible locations of the landmarks, and then apply a nearest neighbor association. However, straight-forward allowance of multiple landmarks with the same signature defeats the huge simplification implicated by having a known data association. Also, such a map representation gives ambiguities in how to present the map to a user and does not use the information that only one of the possible positions are valid at each point in time.

A. Multi-Hypothesis Map

This section presents a multi-hypothesis map representation where different discrete positions of a landmark are all included in the map but grouped together based on their signature. A landmark observation is via a unique identifier associated to a specific group in the map. Within each group the landmark position with highest probability according to incoming observations can be selected as active. By marking all other landmarks in the same group as inactive at the time, a valid up-to-date version of the map can be obtained.

Define the multi-hypothesis map by

$$\mathcal{M} = \left\{ m_1^{s_1}, \dots, m_{n_{s_1}}^{s_1}, \dots, m_1^{s_k}, \dots, m_{n_{s_k}}^{s_k} \right\}, \quad (3)$$

where s_j implies that the landmark belongs to group j, with a total number of k groups. A version of a specific landmark will be referred to as a mode and the number of possible modes of the landmark with signature s_j is thus given by n_{s_j}. Let $\delta^j = q$, $q \in \{1, \dots, n_{s_j}\}$ define a mode indicator for the landmarks in the group s_j, stating that landmark $m_q^{s_j}$ is active.

A mode indicator vector can then be constructed for each time instance t,

$$\delta_t = \begin{bmatrix} \delta_t^1 & \dots & \delta_t^k \end{bmatrix}^\top, \tag{4}$$

indicating which mode is active in each landmark group at a particular point in time. This yields a sequence of mode vectors in time,

$$\delta_{1:T} = \{\delta_1, \dots, \delta_T\}. \tag{5}$$

The non-static map can now be represented by a static part $\mathcal{M}$ and a sequence of mode vectors $\delta_{1:T}$, stating which landmarks contained in $\mathcal{M}$ are active at each time instance.

The mode sequence is modeled by a discrete valued Markov chain with a time dependent transition matrix. For group j the elements in the transition matrix Π_{t-1}^j is defined by,

$$\Pr(\delta_t^j = k | \delta_{t-1}^j = q) = \left[\Pi_{t-1}^j\right]_{qk}, \tag{6}$$

where $[\cdot]_{qk}$ is the element in the qth row and kth column. If the modes for the different landmark groups are assumed independent the full Markov chain factorizes by

$$\Pr(\delta_t | \delta_{t-1}) = \prod_{j=1}^{k} \Pr(\delta_t^j | \delta_{t-1}^j), \tag{7}$$

A map with this representation could be created, with slight adaptions, by a standard *simultaneous localization and mapping* (SLAM) system or manually obtained from prior measurements. A SLAM based mapping can provide a full covariance matrix of the landmarks, whereas with a more manual approach it is at least possible to estimate the uncertainty for individual landmarks. Knowledge about the uncertainty in the map improves the quality of the estimate of the mode sequence, as seen later in the simulation study. Therefore a covariance matrix associated with the map $R_{\mathcal{M}}$, is included as part of the map representation.

B. Multi-Hypothesis State Estimation

With the multi-hypothesis map representation, the observation model is extended to

$$p(z_t | x_t, \mathcal{M}, \delta_t), \tag{8}$$

conditioning also on the current active mode. The full state estimation problem now constitutes estimating the joint distribution,

$$p(x_{1:T}, \delta_{1:T} | \mathcal{M}, z_{1:T}), \tag{9}$$

where $u_{1:T}$ are from now on omitted to simplify the notation. The filtering problem can be formulated as estimating

$$p(x_T, \delta_T | \mathcal{M}, z_{1:T}), \tag{10}$$

which can be split into two factors

$$p(x_T, \delta_T | z_{1:T}, \mathcal{M}) = p(x_T | z_{1:T}, \delta_T, \mathcal{M}) p(\delta_T | z_{1:T}, \mathcal{M}). \tag{11}$$

The first factor constitutes the static state estimation problem conditioned on a mode vector. The second factor is the likelihood of the mode vector conditioned on the sequence of measurements.

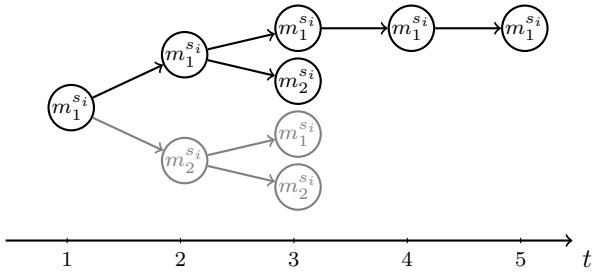

Fig. 2. Possible mode sequences for one landmark with two different mode possibilities at each time instance. At $t = 4$ mode 1 is deduced and the number of mode sequences that has to be continued is reduced to one.

Estimating (11) is in theory possible by associating one filter instance to each possible mode sequence and at the same time estimate the probability of that particular sequence. However, this quickly becomes computationally intractable since the number of mode sequences explodes and depending on the application running one filter can be challenging enough. Fig. 2 shows how the number of mode sequences increases exponentially for only one landmark group with two modes. If it is possible to deduce which mode is active at one specific time instance the tree of growing number of mode sequences can be halved. If then also the assumption of a non-static environment (where landmarks does not move while in field-of-view) is exploited, the number of mode sequences can be reduced to one. The time dependent transition matrix is set to identity when a landmark is in field-of-view to defer any hypotheses growth until the area is revisited.

When a landmark is not in field-of-view the probabilities are of no practical interest from the state estimation perspective. The probabilities can therefore be updated once, when the landmark enters field-of-view, assuming that the transition matrix is constant during the time window when the landmark is not visible,

$$\Pr(\delta_{t+i}^j) = \widetilde{\Pi}^j \Pr(\delta_t^j) = \left(\Pi_t^j\right)^i \Pr(\delta_t^j). \tag{12}$$

Note that if providing online map information is a priority, this simplification should not be used.

IV. Hypothesis Score

This section defines a hypothesis score used to determine which mode is active for a specific landmark group at a particular visit. The hypothesis score is updated each time a new observation is available and a decision is taken if the score passes a threshold.

A. Hypothesis Score Definition

Consider a landmark during a time window $t \in [t_1, t_2]$ where the landmark is in field-of-view. Define the hypothesis that the landmark with signature s_j, is located in one of the positions,

$$\mathcal{H}_k^j : \delta_t^j = k, \quad \forall\, t \in [t_1, t_2]. \tag{13}$$

Consider the log-likelihood of the hypothesis conditioned on observations and apply Bayes' rule,

$$L_t^{\mathcal{H}_k^j} = \log \Pr(\mathcal{H}_k^j | z_{t_1:t}) = \log \frac{p(z_{t_1:t} | \mathcal{H}_k^j) \Pr(\mathcal{H}_k^j)}{p(z_{t_1:t})}. \tag{14}$$

A *hypothesis score* is then defined as

$$L_t^{\mathcal{H}_{ki}^j} = \log \frac{\Pr(\mathcal{H}_k^j|z_{t_1:t})}{\Pr(\mathcal{H}_i^j|z_{t_1:t})} = \log \frac{p(z_{t_1:t}|\mathcal{H}_k^j)\Pr(\mathcal{H}_k^j)}{p(z_{t_1:t}|\mathcal{H}_i^j)\Pr(\mathcal{H}_i^j)}, \quad (15)$$

where the normalizing constant $p(z_{t_1:t})$ cancels. The marginal probability of a hypothesis $\Pr(\mathcal{H}_k^j)$ can be deduced from the Markov chain,

$$\Pr(\mathcal{H}_k^j) = \Pr(\delta_t^j = k, \delta_{t-1}^j = k, \ldots, \delta_{t_1}^j = k) = \Pr(\delta_t^j = k|\delta_{t-1}^j = k)\Pr(\delta_{t-1}^j = k). \quad (16)$$

The first factor in the last equality comes from the Markov chain transition matrix Π_{t-1}^j, and since the landmark is in field-of-view Π_{t-1}^j is identity and,

$$\Pr(\delta_t^j = k) = \Pr(\delta_{t-1}^j = k) = \ldots = \Pr(\delta_{t_1}^j = k). \quad (17)$$

For times before $t = t_1$ the transition matrix is generally not identity and $\Pr(\delta_{t_1}^j = k)$ is computed according to the transition probabilities in $\Pi_{t_1-1}^j$ (or $\widetilde{\Pi}^j$ if (12) is used) and prior knowledge of the mode from previous visits $\Pr(\delta_{t_1-1}^j = i)$,

$$\Pr(\delta_{t_1}^j = k) = \sum_i \Pr(\delta_{t_1}^j = k|\delta_{t_1-1}^j = i)\Pr(\delta_{t_1-1}^j = i). \quad (18)$$

Assuming the measurements in the sequence $z_{t_1:t}$ are mutually independent, the unnormalized log-likelihood $\hat{L}_t^{\mathcal{H}_k^j} \propto L_t^{\mathcal{H}_k^j}$ can be updated recursively as new measurements become available,

$$\hat{L}_t^{\mathcal{H}_k^j} = \hat{L}_{t-1}^{\mathcal{H}_k^j} + \log p(z_t|\mathcal{H}_k^j), \quad (19)$$

$$\hat{L}_{t_1}^{\mathcal{H}_k^j} = \log p(z_{t_1}|\mathcal{H}_k^j)\Pr(\delta_{t_1}^j = k). \quad (20)$$

Hypothesis scores can thus be computed by taking differences of unnormalized log-likelihoods,

$$L_t^{\mathcal{H}_{ki}^j} = \hat{L}_t^{\mathcal{H}_k^j} - \hat{L}_t^{\mathcal{H}_i^j}. \quad (21)$$

If only two modes are present in the map ($n_{s_j} = 2$), a decision can be made according to a *sequential probability ratio test* (SPRT) [18],

$$\log \frac{\beta}{1-\alpha} \leq L_t^{\mathcal{H}_{21}^j} \leq \log \frac{1-\beta}{\alpha}, \quad (22)$$

where α and β are the type 1 and type 2 error probabilities, respectively, and are given by the application. Due to the recursive score update it is possible to make a decision before reaching $t = t_2$. In situations with more than two modes a multi-hypothesis SPRT can be used. All pair-wise scores, $L_t^{\mathcal{H}_{ki}^j}$, are computed and a decision is made in favor of $\mathcal{H}_k^j$ if,

$$L_t^{\mathcal{H}_{ki}^j} > \frac{1-\alpha}{\alpha} \quad \text{for all } i \neq k, \quad (23)$$

where α is the accepted probability of selecting the wrong hypothesis [19].

Note that the probability of a hypothesis can be acquired from the score directly if $n_{s_j} = 2$, or, by solving a system of equations containing the scores if $n_{s_j} > 2$.

B. Multiple Group Evaluations

In a map with more than one group, there might be situations where multiple groups are evaluated simultaneously. The likelihoods for the recursive update in (19) can then be obtained by marginalization over the modes in the other groups,

$$p(z_t|\mathcal{H}_k^j) = \sum_{q^{\mathcal{E}}} p(z_t|\delta_t^j = k, \delta_t^{\mathcal{E}} = q^{\mathcal{E}})\Pr(\delta_t^{\mathcal{E}} = q^{\mathcal{E}}), \quad (24)$$

where $\delta_t^{\mathcal{E}}$ are the set of mode indicators for all other groups than j such that $\{\delta_t^j, \delta_t^{\mathcal{E}}\} = \delta_t$, $q^{\mathcal{E}}$ is one possible realization of $\delta_t^{\mathcal{E}}$, and the summation is over all possible $q^{\mathcal{E}}$. The probabilities $\Pr(\delta_t^{\mathcal{E}} = q^{\mathcal{E}})$ are given by the Markov chain as described in (16) and (17) causing terms for groups not currently under evaluation to be zero.

Another possibility is to define a single hypothesis as a realization of the complete mode vector, with decision made according to the multi-hypothesis SPRT in (23). However, the former approach of marginalization has the benefit of providing mode probabilities for each group individually at all time steps, which makes it more appealing since providing map information is part of the problem statement. Therefore the marginalization approach is the one pursued in this paper.

C. Measurement Likelihood

In a perfect world, computations of the measurement likelihoods $p(z_t|\mathcal{H}_k^j)$ are explicitly given by the filter algorithm. In reality, sensors provide noisy data and methods for extracting landmarks from raw data increases the uncertainty further. This section presents how a realistic value of the likelihoods can be computed inspired by target tracking applications.

Assume that each landmark $m_k^{s_j}$ in the map has a probability of detection given by,

$$P_{\mathrm{D}}^{jk}(x_t) = P_{\mathrm{D0}} P_{\mathrm{FOV}}^{jk}(x_t), \quad (25)$$

where P_{D0} is a sensor specific part, modeled by sensor type specific models or as a constant [20]. Also the uncertainty from the landmark extraction method of choice is included in P_{D0}. The probability that a landmark is in field-of-view is given by $P_{\mathrm{FOV}}^{jk}(x_t)$, as a function of the state vector. With a filtering approach, the state vector and its uncertainty is estimated, which in combination with the uncertainty of the landmarks, $R_{\mathcal{M}}$, determines $P_{\mathrm{FOV}}^{jk}(x_t)$. Clutter, consisting of spurious measurements not originating from any known landmark, is assumed Poisson distributed, with a false alarm rate β_{FA}.

In target tracking, the hypothesis likelihood is factorized with the assumption that observations of different targets/landmarks are independent. This is not valid if the map covariance $R_{\mathcal{M}}$ contains known landmark correlations. However, a reasonable assumption is that clutter and missed detections are independent from observations matched to landmarks

in the map. Assuming only one group is currently evaluated, the likelihood can be factorized as,

$$p(z_t|\mathcal{H}_k^j) = P_{D0}^{|\mathcal{J}|}\left(\prod_{j\in\mathcal{J}} P_{\mathrm{FOV}}^{jk}\right) p(z_t^{\mathcal{J}}|\mathcal{H}_k^j) \times \beta_{\mathrm{FA}}^{m_t^{\mathrm{FA}}} \prod_{j\in\mathcal{M}_D}\left(1 - P_{D0}P_{\mathrm{FOV}}^{jk}\right), \quad (26)$$

where $z_T^{\mathcal{J}}$ is the sub-set of the measurements in the scan z_t that are matched to a landmark in the map, $|\mathcal{J}|$ is the cardinality of $z_T^{\mathcal{J}}$, $\mathcal{M}_D$ is the set of missed detections (*i.e.*, landmarks with $P_{\mathrm{FOV}} > 0$ that are not represented in the observations). The number of false alarms are denoted by m_t^{FA}.

Let z_t^j denote the element in the measurement vector associated with group s_j, and let $z_t^{\mathcal{E}}$ denote all other measurements associated with other landmarks such that $\{z_t^j, z_t^{\mathcal{E}}\} = z_t^{\mathcal{J}}$. The number of false alarms m_t^{FA}, the set of missed detections $\mathcal{M}_D$, and the field-of-view probabilities (also for landmarks not in group j) might be different among the hypotheses since each hypothesis is associated with its own state estimate. However, in the first update when the hypothesis is branched the state estimate is equal for all hypotheses and it is enough to compute,

$$p(z_t|\mathcal{H}_k^j) \propto \begin{cases} P_{D0}P_{\mathrm{FOV}}^{jk} p(z_t^{\mathcal{J}}|\mathcal{H}_k^j) & \text{if } z_t^j \neq \emptyset \\ (1 - P_{D0}P_{\mathrm{FOV}}^{jk}) p(z_t^{\mathcal{E}}|\mathcal{H}_k^j) & \text{if } z_t^j = \emptyset, \end{cases} \quad (27)$$

since all other factors cancels when the pair-wise hypothesis score is formed. This formulation can be used also for further updates, as an approximation of (26), if the state estimates associated with the different hypothesis are close to each other, or if the application has computational limitation.

In the single group case the likelihoods $p(z_t^{\mathcal{J}}|\mathcal{H}_k^j)$, $p(z_t^{\mathcal{E}}|\mathcal{H}_k^j)$, and, P_{FOV}^{jk} are directly given by the single state estimator associated with the hypothesis. If many groups are evaluated simultaneously, multiple state estimators are associated with the hypothesis $\delta^j = k$ and the likelihoods have to be computed with marginalization according to (24).

V. Hypothesis Score Localization

This section describes how the multi-hypothesis map representation and score based decision making can be utilized for state estimation. A workflow is presented where a filter algorithm provides an estimate of $p(x_t|z_{1:t}, \delta_t, \mathcal{M})$ and $p(\delta_t|z_{1:t}, \mathcal{M})$ is obtained by a *map update*.

A map $\mathcal{M}$, with associated covariance matrix $R_{\mathcal{M}}$, is given at initialization together with an initial state x_0, and state covariance P_0. A single state estimator is created on initialization and added to a list of hypothesis filters, $\mathcal{F}$. When new observations are available, all filters in the list is predicted to time t by the state transition model, then a *map update* is done by computing hypothesis scores for all landmarks in field-of-view, possibly adding or removing filters from the hypothesis list. Finally, a standard filter measurement update is performed on all filters in the list based on their associated mode vector. A single state estimate can be obtained from the filter associated with the most current map information. In Algorithm 1 the workflow is described in pseudo code, and the map update is performed on the lines 6–28.

Algorithm 1 Multi-Hypothesis Localization

Input: $\mathcal{M}$, $R_{\mathcal{M}}$, $\mathcal{S} = \emptyset$, $\mathcal{F} = \emptyset$, x_0, P_0, $u_{1:T}$, $z_{1:T}$
1: Initialize filter (x_0, P_0) and add to $\mathcal{F}$
2: **for** t = 1:T **do**
3: **for all** filters in $\mathcal{F}$ **do**
4: $(\tilde{x}_t, \tilde{P}_t) \leftarrow$ filter predict$(\hat{x}_{t-1}, \hat{P}_{t-1}, u_t)$
5: **end for**
6: **for all** landmarks $m_k^{s_j}$ in $\mathcal{M}$ **do**
7: Compute $P_{\mathrm{FOV}}^{jk}(\tilde{x}_t, \tilde{P}_t)$
8: **if** $P_{\mathrm{FOV}}^{jk} > \gamma$ and $j \notin \mathcal{S}$ **then**
9: $\hat{L}_t^{\mathcal{H}_k^j} \leftarrow$ initialize according to (20)
10: Add j to $\mathcal{S}$ and associated filters to $\mathcal{F}$
11: **else if** $P_{\mathrm{FOV}}^{jk} < \gamma$ and $j \in \mathcal{S}$ **then**
12: $\Pr(\delta_t^j) \leftarrow$ compute from score
13: Remove j from $\mathcal{S}$ and associated filters from $\mathcal{F}$
14: **end if**
15: **end for**
16: **for all** $j \in \mathcal{S}$ **do**
17: $\hat{L}_t^{\mathcal{H}_k^j} \leftarrow$ update according to (19)
18: **if** decision is made in favour of hypothesis $\mathcal{H}_q^j$ **then**
19: $\hat{\delta}_t^j = q$
20: $\Pr(\delta_t^j = q) = 1$, $\Pr(\delta_t^j \neq q) = 0$
21: Remove j from $\mathcal{S}$ and associated filters from $\mathcal{F}$
22: **else**
23: $\hat{\delta}_t^j = \max_k L_t^{\mathcal{H}_k^j}$
24: **end if**
25: **end for**
26: **for all** $j \notin \mathcal{S}$ **do**
27: $\hat{\delta}_t^j = \hat{\delta}_{t-1}^j$
28: **end for**
29: **for all** filters in $\mathcal{F}$ **do**
30: $(\hat{x}_t, \hat{P}_t) \leftarrow$ filter correct$(\tilde{x}_{t-1}, \tilde{P}_{t-1}, z_t)$
31: **end for**
32: $(\hat{x}_t^G, \hat{P}_t^G) \leftarrow$ from filter associated with $\hat{\delta}_t$
33: **end for**
Output: $\hat{x}_{1:T}^G$, $\hat{P}_{1:T}^G$, $\hat{\delta}_{1:T}$

A. Map Update

For book keeping, it is convenient to keep a list of groups in the map currently under evaluation, $\mathcal{S}$. When the probability that a landmark is in field-of-view goes above a threshold, γ, the null hypothesis scores for all landmarks in that group is initialized according to (20), and the group is added to $\mathcal{S}$. New filters associated with the newly appearing hypothesis are created and added to $\mathcal{F}$. The number of filter that has to be created depends on the number of groups already in $\mathcal{S}$.

The hypothesis score is then updated for all groups in $\mathcal{S}$ by using (26) or (27). This update either uses the observation associated to a specific group, or the scores are updated with the negative information that an expected observation is missing. A *maximum likelihood* (ML) estimate of the mode indicator vector $\hat{\delta}_t$ can be acquired by selecting the landmark in each group with highest score. If a decision according to (22) or (23) can be made for landmarks in group i, after the scores are updated, the mode indicator is set to the decided landmark, $\delta_t^i = q$ and the group is removed from $\mathcal{S}$, to prevent unnecessary score computations until next time the landmarks enter field-of-view. The likelihood that another mode is active is now considered to be zero, $\Pr(\delta_t^i \neq q) = 0$.

A situation may occur where a landmark leaves field-of-view before a decision has been made. (This corresponds to line 12 in Algorithm 1.) The state estimator to continuate can then either be chosen according to ML or by merging the associated state hypotheses.

VI. Simulations

This section presents simulated experiments highlighting different aspects and benefits of the proposed multi-hypothesis approach. Experiments are performed in two different environments, one open area environment illustrating the concepts of the multi-hypothesis approach presented in Algorithm 1, and one of an office corridor where uniquely identifiable landmarks are placed on walls and door handles. This environment shows how the multi-hypothesis map representation can be used in a more realistic scenario and is also used to demonstrate how the estimate benefits from utilizing information about uncertainties in the map.

A. Data Generation

The state vector consists of Cartesian coordinates in combination with the heading of the robot $x_t = [x^1, x^2, \theta]^\top$. Along a trajectory, noisy measurements of the linear and angular velocities are simulated, comprising,

$$u_t = \begin{bmatrix} u_t^v \\ u_t^\omega \end{bmatrix} + \begin{bmatrix} e_t^v \\ e_t^\omega \end{bmatrix}, \tag{28}$$

where $e_t^v \sim \mathcal{N}(0, 0.1^2)$ and $e_t^\omega \sim \mathcal{N}(0, (5^\circ)^2)$ are noise added to the linear and angular velocity, respectively. Landmark observations are simulated along the same trajectory by transforming visible landmarks in the map, given in the global coordinate frame, to points in the robots coordinate frame. Which yields the observation model,

$$z_t = \mathcal{R}(x_t)\left(\mathcal{M}_V - x_t^{(1,2)}\right) + e_t^m, \tag{29}$$

where $\mathcal{R}(x_t)$ is a rotation matrix, $x_t^{(1,2)}$ are the Cartesian components of the state vector, and, $\mathcal{M}_V$ is the subset of the complete map $\mathcal{M}$ containing landmark positions that are currently true and that are within the robot's field-of-view. The measurement noise is additive and white Gaussian, $e_t^m \sim \mathcal{N}(0, R_S)$, with $R_S = aI$ with scalar a and I is the identity matrix. The observations are simulated with a probability of detection $P_D = 0.9$ and clutter with a rate β_{FA}, with $\beta_{\text{FA}} V = 0.01$, where V is the area of the field-of-view of the robot. The field-of-view is a disc with radius 3 m.

To simulate an actual uncertainty in the landmark position in the map, all measurements are simulated with the true positions of all landmarks, while the localization system is given a sample from the distribution $\widetilde{\mathcal{M}} \sim \mathcal{N}(\mathcal{M}, R_\mathcal{M})$. The diagonal of $R_\mathcal{M}$ is set to 0.006 and covariances to 0.002 for all landmarks in different groups. Covariances for landmarks within the same group are set to zero. The order of magnitude of these uncertainties are obtained from the outcome of a SLAM simulation in the corridor environment.

B. State Estimator

A UKF is implemented for the static localization utilizing the state transition model,

$$x_t = x_{t-1} + T \begin{bmatrix} u_t^v \cos\theta_t \\ u_t^v \sin\theta_t \\ u_t^\omega \end{bmatrix} + v_t, \tag{30}$$

where $T = 50\,\text{ms}$ is the sampling rate and the process noise $v_t \sim \mathcal{N}(0, Q)$ is modeled as time-invariant with diagonal covariance $Q = 0.05\text{diag}(0.1^2, 0.1^2, (5^\circ)^2) + \text{diag}(0.0002, 0.000.2, 0)$, where the extra term is to compensate for the nonlinearity in the first two components in the state transition model. The UKF is implemented with symmetric sigma point selection and standard parameter values, $\alpha = 10^{-3}$, $\beta = 2$, and, $\kappa = 0$ according to [21].

For the mode probabilities the single update in (12) is used with a constant $\widetilde{\Pi}^j = \left[\begin{smallmatrix} 0.9 & 0.1 \\ 0.1 & 0.9 \end{smallmatrix}\right] \forall j$, regardless of the length of the time window the landmark has been non-visible for.

The field-of-view probability P_{FOV}^{jk} of a landmark is estimated by sampling from the landmark distribution $\mathcal{N}(m_k^{s_j}, R_\mathcal{M}^{jk})$ and the current state estimate $\mathcal{N}(\hat{x}_t, \hat{P}_t)$, and compute the ratio of samples where the landmark is visible. The visibility threshold is set to $\gamma = 0.8$. The approximation of the measurement likelihood in (27) is used and $p(z_t^\mathcal{J}|\mathcal{H}_k^j)$ are obtained by transforming the observations, given in the robot's sensor coordinate frame, to the global frame of the landmark in the map. Given the observation model (29) this yields,

$$z_t^{\text{global}} \sim \mathcal{N}(\mathcal{R}^{-1}(x_t) z_t^{\text{local}} + x_t, \mathcal{R}^{-1}(x_t) R (\mathcal{R}^{-1}(x_t))^\top). \tag{31}$$

The likelihood is computed by forming the distribution of the difference between z_t^{global} and the visible landmarks in the map, $\widetilde{\mathcal{M}}_V$, and evaluate the probability density function at the residuals, $r_t = z_t^{global} - \widetilde{\mathcal{M}}_V$,

$$p(z_t|\mathcal{H}_k^j) = \frac{1}{\sqrt{(2\pi)^{\dim(z_t)} \det S}} e^{\left(-\frac{1}{2} r_t^\top S^{-1} r_t\right)}, \tag{32}$$

where $S = R_{\mathcal{M}_V} + \mathcal{R}^{-1}(x_t) R \left(\mathcal{R}^{-1}(x_t)\right)^\top$, and $R_{\mathcal{M}_V}$ is the elements in $R_\mathcal{M}$ corresponding to the currently visible landmarks.

C. Open Area Environment

In the open area environment two landmarks are present and a robot is moving towards them in a straight line starting far enough away for the landmarks not to be in field-of-view. One of the landmarks have two possible locations with $m_1^{s_1}$ marked in Fig. 3 corresponding to the truth. The measurement noise is set to a rather high level ($a = 0.5$) causing bad separation between the constructed mode hypotheses. The modes are initialized with equal probability 0.5, and in Fig. 3 the estimated trajectory is given as well as the final probabilities of the landmark modes. Fig. 4 shows the hypothesis score for the two modes of landmark 1 for each time step. At $t = t_1$ the hypothesis score is initialized as 0 since both hypothesis are equally likely. This creates an alternative state estimator (the grey line in Fig. 3). Due to the bad separation, only

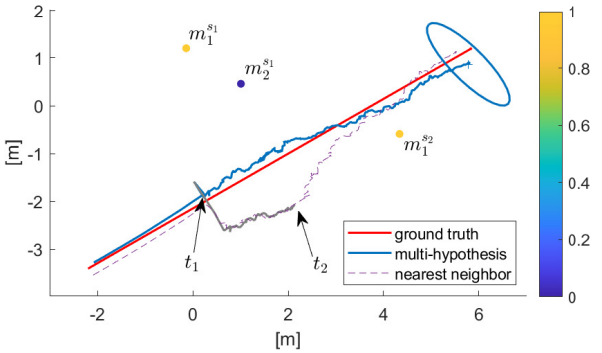

Fig. 3. The blue line shows the estimated trajectory with the uncertainty ellipse at the final time step, the red line is the true trajectory and the grey line is the rejected hypothesis. The purple dashed line is the nearest neighbor trajectory estimate. Landmarks are marked with colored dots where the colorbar indicates the estimated probability of existence of the landmarks at the final time step.

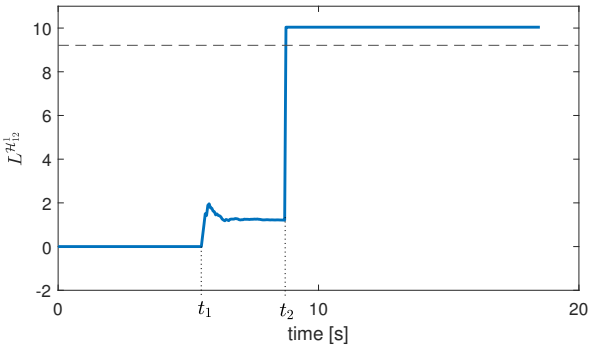

Fig. 4. The hypothesis score $L^{\mathcal{H}^1_{21}}$ for the landmarks in group s_1 in Fig. 3. At $t = t_1$ the hypothesis score is initialized and at $t = t_2$ also the single hypothesis landmark in group s_2 comes into field-of-view increasing the probability of $\delta^1 = 1$. The dashed line marks the threshold in the SPRT test.

receiving measurements from landmark 1 is not enough to make a decision. However at $t = t_2$, landmark 2 comes into field-of-view and the wrong hypothesis is immediately rejected when the score goes above the threshold marked in Fig. 4. As soon as the threshold is passed, the score is not updated anymore and hence the value is constant for $t > t_2$.

Fig. 3 also shows the trajectory estimate with a nearest neighbor approach, where the filter in each time update selects the landmark mode closest to current measurement. This gives an estimated trajectory following one of the two hypothesis, but which one is not deterministic and depends on which landmark the first measurement happens to be closest to.

D. Corridor Environment

The corridor environment represents an office where uniquely identifiable landmarks are placed on walls and door handles. In this setting the different modes constitutes situations where the doors are open or closed, causing these landmarks to have possibly two discrete positions. For simulations in this environment $a = 0.01$ is used in the measurement noise.

A standard static map localization, where only one of the options of the door handle position is represented in the map, results in an inconsistent state estimate when the door

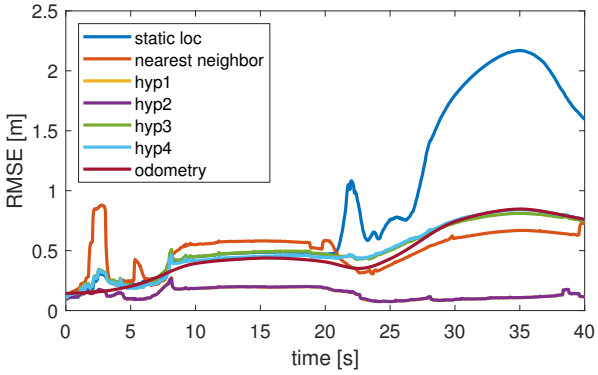

Fig. 5. The RMSE of 1000 MC realizations of the trajectory state estimation. Results are given for four different utilization levels of the map uncertainty when adopting the multi-hypothesis map representation. Also the results of a static localization assuming all doors are always opened, a nearest neighbor solution, and a pure odometric dead-reckoning localization are presented. (Note that *hyp1* is almost completely hidden by *hyp2*.)

TABLE I
AVERAGE NEES VALUES OVER THE TRAJECTORY STATE ESTIMATION. BOTH THE MEAN AND THE MEDIAN OF 1000 MC REALIZATIONS ARE GIVEN. THE RESULTS ARE FOR THE SAME ESTIMATION METHODS AS PRESENTED IN FIG. 5, WITH AN OPTIMAL NEES VALUE OF 3.

NEES	static loc	nearest neighbor	hyp1	hyp2	hyp3	hyp4	odo-metry
mean	1330	775	7.5	8.1	220	224	0.89
median	1290	690	4.5	4.8	107	106	0.48

handle positions have changed, see Fig. 1. If instead the multi-hypothesis map representation is used for the same problem, hypothesis are re-evaluated when a door has been opened or closed causing incoming observations to be associated with the landmark with correct position in the map. Fig. 1 shows the estimated trajectory and the likelihood of landmark positions at the final time step using Algorithm 1.

The uncertainty in the map $R_{\mathcal{M}}$ is used in the map update to get good estimates of the field-of-view probability and measurement likelihood. However, knowledge about the map uncertainty can also be utilized to improve the performance of the static localization process. In the simulation depicted in Fig. 1, the measurement noise covariance provided to the UKF is boosted by the known landmark position uncertainty. Instead of just providing R_S as measurement noise, $R_S + \mathcal{R}(x_t) R_{\mathcal{M}_V} \mathcal{R}^\top(x_t)$ is given at each time step, according to (29).

Fig. 5 shows the *root mean square error* (RMSE), and Table I the average *normalized estimated error squared* (NEES), for 1000 *Monte Carlo* (MC) realizations of the trajectory simulation, for different utilization levels of the map uncertainty. The levels are given in descending order of information utilization.

- *hyp1*: The map covariance information $R_{\mathcal{M}}$, is utilized both in the mode decision making and in the static filter update.
- *hyp2*: Only the diagonal elements of $R_{\mathcal{M}} = 0$ are used for decision making and filter update, neglecting the correlations between landmarks.
- *hyp3*: $R_{\mathcal{M}}$ is only used for mode decision making not for

TABLE II
RATIO OF MODE DECISIONS TAKEN FOR DIFFERENT UTILIZATION LEVELS OF THE MAP UNCERTAINTY INFORMATION IN THE CORRIDOR ENVIRONMENT.

Method	Correct decision	Wrong decision	No decision
hyp1	96.5%	1.6%	1.9%
hyp2	96.4%	1.6%	2.0%
hyp3	95.0%	1.8%	3.2%
hyp4	94.4%	1.7%	3.9%

boosting the measurement noise provided to the UKF.

- *hyp4*: No map covariance information is used at all ($R_{\mathcal{M}} = 0$).

The NEES is computed by $(x_t - \hat{x}_t)^\top \hat{P}_t^{-1} (x_t - \hat{x}_t)$, where x_t are the true state vector. For Gaussian distribution of the state, this quantity is χ^2-distributed and the optimal value is equal to the dimension of the state vector [22].

In general, the more the information about the map uncertainty is utilized the better the estimate. However, including the correlation between the landmarks does not significantly improve the result (*hyp1* and *hyp2* are almost overlapping in Fig. 5). All utilization levels results in a optimistic estimate according to the NEES measure. One explanation for this is the relatively few landmarks in this environment. In each realization a new map $\widetilde{\mathcal{M}}$ is sampled. In realizations where a landmark that is the only visible landmark for a long period of time, happens to be placed far away from the mean value, the state estimate is overcompensating for measurement from this landmark. This results in very optimistic NEES values for this specific realization, which increases the mean over all realizations. If instead the median of the NEES values is considered over the realization, the average NEES value over the trajectory are closer to the optimal value for *hyp1* and *hyp2*.

Using the uncertainty for mode decision making does not give a huge improvement in the average position estimation error but the ratio of correct mode decisions taken increases, see Table II where the ratios of decisions taken for the different methods are presented.

VII. CONCLUSION

This paper considered the problem of position estimation in non-static environments with uniquely identifiable landmarks. A feature based multi-hypothesis map representation has been presented where each feature can be associated with multiple discrete positions in the map. To deduce which hypothesis is currently active, a hypothesis score is defined which enables a decision to be made and reduces the otherwise exponential growth of the hypothesis tree.

Simulation experiments have been conducted to show the benefit of including the uncertainty in the landmarks positions in the map representation. This increases the quality of the state estimates while at the same time providing up-to-date information about actual landmark positions.

Future work will be to investigate how maps with the suggested representation can automatically be created within the SLAM framework. This will also allow the set of landmarks within the map to be dynamic.

REFERENCES

[1] S. Thrun, W. Burgard, and D. Fox, *Probabilistic robotics*. MIT Press, 2005.

[2] L. Bernreiter, A. R. Gawel, H. Sommer, J. Nieto, R. Siegwart, and C. C. Lerma, "Multiple hypothesis semantic mapping for robust data association," *IEEE Robotics and Automation Letters*, pp. 1–1, 2019.

[3] T. Ran, L. Yuan, J. Zhang, L. He, R. Huang, and J. Mei, "Not only look but infer: Multiple hypothesis clustering of data association inference for semantic SLAM," *IEEE Transactions on Instrumentation and Measurement*, vol. 70, pp. 1–9, 2021.

[4] P. Biber and T. Duckett, "Dynamic maps for long-term operation of mobile service robots," in *Robotics: Science and Systems I*, jun 2005, pp. 17–24.

[5] ——, "Experimental analysis of sample-based maps for long-term SLAM," *The International Journal of Robotics Research*, vol. 28, no. 1, pp. 20–33, jan 2009.

[6] W. Churchill and P. Newman, "Practice makes perfect? Managing and leveraging visual experiences for lifelong navigation," in *Proc. Int. Conf. on Robotics and Automation*. Saint Paul, USA: IEEE, may 2012, pp. 4525–4532.

[7] K. Konolige and J. Bowman, "Towards lifelong visual maps," in *Proc. Int. Conf. on Intelligent Robots and Systems*, St. Louis, MO, USA, 2009, pp. 1156–1163.

[8] K. Konolige, J. Bowman, J. D. Chen, P. Mihelich, M. Calonder, V. Lepetit, and P. Fua, "View-based maps," *The International Journal of Robotics Research*, vol. 29, no. 8, pp. 941–957, 2010.

[9] A. Walcott-Bryant, M. Kaess, H. Johannsson, and J. J. Leonard, "Dynamic pose graph SLAM: Long-term mapping in low dynamic environments," in *Proc. Int. Conf. on Intelligent Robots and Systems*, Vilamoura, Portugal, 2012, pp. 1871–1878.

[10] D. Meyer-Delius, M. Beinhofer, and W. Burgard, "Occupancy grid models for robot mapping in changing environments," in *Proc. AAAI Conf. on Artificial Intelligence*, 2012, pp. 2024–2030.

[11] J. Saarinen, H. Andreasson, and A. J. Lilienthal, "Independent markov chain occupancy grid maps for representation of dynamic environment," in *Proc. Int. Conf. on Intelligent Robots and Systems*, Vilamoura, Portugal, 2012, pp. 3489–3495.

[12] T. Morris, F. Dayoub, P. Corke, G. Wyeth, and B. Upcroft, "Multiple map hypotheses for planning and navigating in non-stationary environments," in *Proc. Int. Conf. on Robotics and Automation (ICRA)*. Hong Kong, China: IEEE, may 2014, pp. 2765–2770.

[13] A. Hornung, K. M. Wurm, M. Bennewitz, C. Stachniss, and W. Burgard, "OctoMap: an efficient probabilistic 3D mapping framework based on octrees," *Autonomous Robots*, vol. 34, no. 3, pp. 189–206, feb 2013.

[14] X. Hu, J. Wang, and W. Chen, "Long-term localization of mobile robots in dynamic changing environments," in *2018 Chinese Automation Congress (CAC)*. IEEE, nov 2018.

[15] D. M. Rosen, J. Mason, and J. J. Leonard, "Towards lifelong feature-based mapping in semi-static environments," in *Proc. Int. Conf. on Robotics and Automation (ICRA)*. Stockholm, Sweden: IEEE, may 2016, pp. 1063–1070.

[16] T. Krajnik, J. P. Fentanes, G. Cielniak, C. Dondrup, and T. Duckett, "Spectral analysis for long-term robotic mapping," in *Proc. Int. Conf. on Robotics and Automation (ICRA)*, Hong Kong, China, 2014, pp. 3706–3711.

[17] R. E. Kalman, "A new approach to linear filtering and prediction problems," *Transactions of the ASME – Journal of Basic Engineering*, vol. 82, pp. 35–45, 1960.

[18] A. Wald, "Sequential Tests of Statistical Hypotheses," *The Annals of Mathematical Statistics*, vol. 16, no. 2, pp. 117–186, 1945.

[19] V. P. Dragalin, A. G. Tartakovsky, and V. V. Veeravalli, "Multihypothesis sequential probability ratio tests .i. asymptotic optimality," *IEEE Transactions on Information Theory*, vol. 45, no. 7, pp. 2448–2461, 1999.

[20] Y. Bar-Shalom, P. K. Willet, and X. Tian, *Tracking and data fusion : a handbook of algorithms*. YBS Publishing, 2011.

[21] E. A. Wan and R. V. D. Merwe, "The unscented Kalman filter for nonlinear estimation," in *Proc. IEEE Adaptive Systems for Signal Processing, Communications, and Control Symposium*, Lake Louise, Alberta, Canada, 2000.

[22] Z. Chen, C. Heckman, S. Julier, and N. Ahmed, "Weak in the NEES?: auto-tuning Kalman filters with Bayesian optimization," in *Proc. 21st Int. Conf. on Information Fusion (FUSION)*, Cambridge, UK, 2018, pp. 1072–1079.